Atmospheric
Chemistry
and Physics

Trajectory model simulations of ozone (O₃) and carbon monoxide (CO) in the lower stratosphere

T. Wang[1], W. J. Randel[2], A. E. Dessler[1], M. R. Schoeberl[3], and D. E. Kinnison[2]

[1]Texas A&M University, College Station, TX, USA
[2]National Center for Atmospheric Research (NCAR), Boulder, CO, USA
[3]Science and Technology Corporation, Lanham, MD, USA

Correspondence to: T. Wang (tao.wang@tamu.edu)

Abstract. A domain-filling, forward trajectory model originally developed for simulating stratospheric water vapor is used to simulate ozone (O₃) and carbon monoxide (CO) in the lower stratosphere. Trajectories are initialized in the upper troposphere, and the circulation is based on reanalysis wind fields. In addition, chemical production and loss rates along trajectories are included using calculations from the Whole Atmosphere Community Climate Model (WACCM). The trajectory model results show good overall agreement with satellite observations from the Aura Microwave Limb Sounder (MLS) and the Atmospheric Chemistry Experiment Fourier Transform Spectrometer (ACE-FTS) in terms of spatial structure and seasonal variability. The trajectory model results also agree well with the Eulerian WACCM simulations. Analysis of the simulated tracers shows that seasonal variations in tropical upwelling exerts strong influence on O₃ and CO in the tropical lower stratosphere, and the coupled seasonal cycles provide a useful test of the transport simulations. Interannual variations in the tracers are also closely coupled to changes in upwelling, and the trajectory model can accurately capture and explain observed changes during 2005–2011. This demonstrates the importance of variability in tropical upwelling in forcing chemical changes in the tropical lower stratosphere.

1 Introduction

The influx of water vapor (H₂O) to the stratosphere is largely determined by the large-scale troposphere-to-stratosphere transport in the tropics, during which air is dehydrated across the cold tropical tropopause (e.g., Fueglistaler et al., 2009, and references therein). Observations such as the entry mixing ratios (Dessler, 1998; Dessler et al., 2013), the coherent relations between water vapor and temperature (Mote et al., 1996), and the extensive cirrus clouds near the tropopause (e.g., Winker and Trepte, 1998; Wang and Dessler, 2012) all support this understanding. Back trajectory models have provided detailed simulations of stratospheric H₂O (e.g., Fueglistaler et al., 2005). More recently, a newly designed domain-filling forward trajectory model driven by reanalysis wind and temperature has demonstrated success at simulating the transport of H₂O in the stratosphere (Schoeberl and Dessler, 2011; Schoeberl et al., 2012, 2013). In this trajectory model, winds determine the pathways of parcels and temperature determines the H₂O content through an idealized saturation calculation. This simple advection–condensation strategy yields reasonable results for H₂O in the stratosphere, although the detailed results depend on the wind and temperature fields utilized and assumptions regarding supersaturation (Liu et al., 2010; Schoeberl et al., 2012).

Besides H₂O, ozone (O₃) and carbon monoxide (CO) are also important trace gases in the stratosphere linked to circulation, transport, and climate forcing (for O₃). Ozone abundances in the stratosphere cover a wide dynamic range (∼ 10s of ppbv to a few ppmv), and are influenced by a variety of chemical and dynamical processes, including photochemical production and loss and large- and small-scale transport (for example, deep convective lofting of boundary layer low-O₃ air to the upper troposphere; e.g., Folkins et al., 2002). CO behaves as a tropospheric source gas, originating from natural and anthropogenic emissions, including combustion

processes near the surface and oxidation of methane and other hydrocarbons within the troposphere. The main sink of CO is oxidation by the hydroxyl radical (OH) (Logan et al., 1981). The CO photochemical lifetime of 2–3 months makes it a useful tracer for transport studies in the troposphere and lower stratosphere (e.g., Bowman, 2006; Schoeberl et al., 2006, 2008).

The purpose of this work is to simulate O_3 and CO in the lower stratosphere using the domain-filling, forward trajectory model used previously for stratospheric H_2O. Trajectory modeling of O_3 and CO can provide useful tests for simplified understanding of transport and chemical processes in the stratosphere, and provide complementary information to the H_2O simulations (which are primarily constrained by tropopause temperatures). In addition to testing circulation and transport within the trajectory model, the O_3 and CO simulations can provide understanding of mechanisms leading to observed chemical behavior, including transport history and pathways, seasonal and interannual variations, and relation to the stratospheric age of air (Waugh and Hall, 2002). Ozone and CO are complementary tracers representing primarily stratospheric and tropospheric sources; both tracers exhibit strong gradients across the tropopause, and they are often combined using tracer correlations to understand transport and chemical behavior in the upper troposphere and lower stratosphere (UTLS) (e.g., Fischer et al., 2000). Furthermore, O_3 and CO exhibit relatively large out-of-phase seasonal cycles in the tropical lower stratosphere (Randel et al., 2007), and these coupled variations provide a sensitive test of the trajectory model simulations in this region.

2 Model description and data used

2.1 Trajectory model

The trajectory model used here follows the details described in Schoeberl and Dessler (2011) and Schoeberl et al. (2012), with trajectories calculated using the Bowman trajectory code (Bowman, 1993; Bowman and Carrie, 2002; Bowman et al., 2013). Because of the overly dispersive behavior of kinematic trajectories (e.g., Schoeberl et al., 2003; Liu et al., 2010; Ploeger et al., 2010; Schoeberl and Dessler, 2011), we perform diabatic trajectories using isentropic coordinates, in which the vertical velocity is the potential temperature tendency converted from the diabatic heating rates via the thermodynamic equation (Andrews et al., 1987).

The methodology for the trajectory simulations of O_3 and CO follows Schoeberl and Dessler (2011) and Schoeberl et al. (2012), wherein the parcels are initialized at the 370 K isentrope, below the tropical tropopause, using climatological O_3 and CO from the Aura Microwave Limb Sounder (MLS, monthly means averaged over 2005–2011) to provide approximate entry level values in the upper troposphere. The

370 K level is chosen as the initialization level because it is above the level of zero net heating rates and parcels there tend to ascend to the stratosphere (see Sect. 5). To account for chemical changes along the trajectories, we use chemical production and loss rates output from the Whole Atmosphere Community Climate Model (WACCM). Specifically, the O_3 and CO concentration carried by each parcel is modified from the previous time step using the production and loss frequencies calculated from WACCM.

For each day 1350 parcels are initiated on an equal area grid covering 40° N–40° S latitude and advected forward in time by reanalysis winds. At the end of each day, any parcels that have descended below the 250 hPa level are removed since in most cases they have re-entered the troposphere. The upper boundary is chosen to be the ~ 2200 K isentrope (~ 1 hPa or ~ 50 km) to cover the entire stratosphere. Parcels are initialized and added to the ensemble consecutively each day and the combined set of parcels is then run forward. This process is repeated over the entire integration period. As more and more parcels are injected into the model, the stratospheric domain is filled up with parcels – this is the concept of domain-filling used in our model. The trajectory model simulations are started in January 1990 and integrated to the end of 2011; after 3–4 years the system reaches steady state with approximately 1 million parcels in the domain. We focus on analyzing the model results during 2005–2011, to overlap the MLS and Atmospheric Chemistry Experiment Fourier Transform Spectrometer (ACE-FTS) observations.

Upwelling across the tropical tropopause in the trajectory model is determined by the reanalysis total diabatic heating rates (Q_{tot}, hereinafter Q), which include heating due to long-wave and short-wave radiation, moist physics, friction, gravity wave drags, etc. As shown below, our simulations of O_3 and CO are sensitive to the imposed upwelling. There is substantial uncertainty in the detailed magnitude and spatial structure of Q, as seen in the differences among separate reanalysis results (Schoeberl et al., 2012; Randel and Jensen, 2013; Wright and Fueglistaler, 2013). Figure 1 illustrates the differences in Q in the tropics (15° N–15° S) based on several reanalysis data sets, highlighting large differences in the UTLS. Given this uncertainty, we tested the sensitivity of our calculations to variations in the heating rates by comparing results based on the NASA Modern Era Retrospective-Analysis for Research and Applications (MERRA; Rienecker et al., 2011) and the ECMWF ERA Interim reanalysis (ERAi; Dee et al., 2011). Below we highlight the sensitivity of the resulting O_3 and CO simulations to these imposed circulations.

Changes in chemical concentrations in the trajectory model are calculated using the chemical continuity equation (e.g., Dessler, 2000):

$$[\chi]_{\text{current}} = [\chi]_{\text{previous}} + \left(P_\chi - \text{LF}_\chi \cdot [\chi]_{\text{previous}} \right) \cdot \Delta t. \quad (1)$$

Here, χ represents either O_3 or CO. Current chemical concentrations $[\chi]_{\text{current}}$ in volume mixing ratio (VMR)
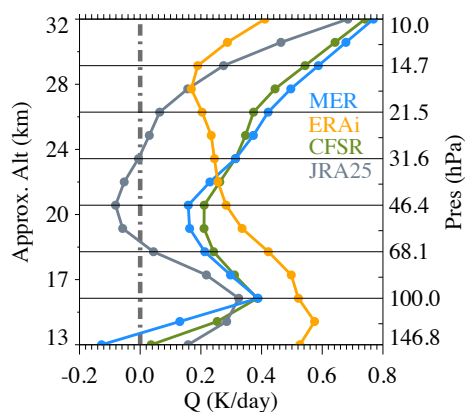
Figure 1. Comparison of total diabatic heating rates averaged over the deep tropics (18° N–18° S) in 2000–2010 from four different reanalysis data sets: MER (MERRA), ERAi (ECMWF ERA interim), CFSR (NCEP CFSR), and JRA25.
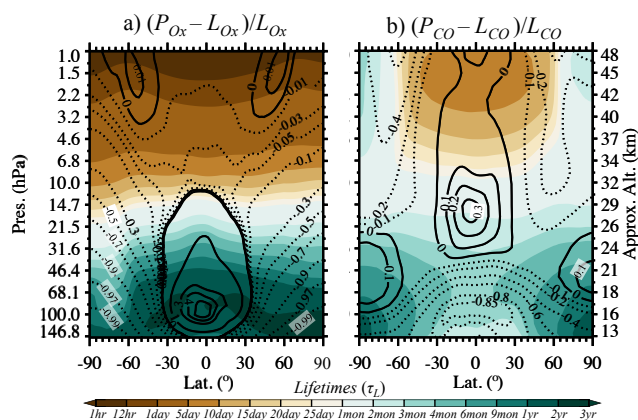

Figure 2. The ratio of chemical net tendency (production rate minus loss rate) to loss rate from WACCM for **(a)** O_x and **(b)** CO. Negative numbers are dashed to highlight the net chemical decrease and positive numbers indicate net chemical increase, while zero lines indicate comparable amount of production and loss. For reference, the respective O_x and CO lifetimes are contoured in color.

are determined by concentrations in previous time step $[\chi]_{previous}$ and the net change, derived from the production minus loss occurring in each time step. The production rate P_χ in VMR per unit time is obtained from WACCM. The loss rate $(LF_\chi \cdot [\chi]_{previous})$ in VMR per unit time is calculated as a product of loss frequency LF_χ (per unit time) times the chemical concentration (VMR), representing a linear chemical loss. The loss frequencies are estimated from WACCM by dividing the model loss rate L_χ by the chemical concentration $[\chi]$, i.e., $LF_\chi = L_\chi / [\chi]$. In our simulation P_χ and LF_χ are calculated from WACCM as a function of latitude, altitude, and climatological months. The time step for calculating trajectories is 45 min while the time step for calculating chemical changes is 1 day.

One advantage of the Lagrangian framework is its ability to trace the full evolution of parcels due to no explicit mixing during the entire trajectory integration. However, there is an effective "mixing" when many parcels are averaged within grid boxes to be compared with either observational or Eulerian model results (see Sect. 3). The mixing in extratropical tropopause is very important, but in this paper we mainly focus our results on the tropical lower stratosphere, where the strong vertical gradients of chemical species indicate less mixing occurring. In fact, it is because Lagrangian models producing nondiffusive transport and thus are especially accurate in regions where there are strong tracer gradients (e.g., the edge of polar vortex, the tropopause).

2.2 WACCM chemical production and loss rates

The chemical production and loss rates from WACCM4 (Garcia et al., 2007) are applied in our model to represent chemical processes. The vertical domain of WACCM4 extends from the surface to the lower thermosphere, with horizontal resolution of $2.5° \times 1.9°$ in longitude and latitude and 88 levels up to $\sim 150\,km$. In the UTLS the vertical resolu-

tion is 1.1–1.4 km. The WACCM4 simulation used here is run with specified dynamics (SD) fields (Lamarque et al., 2012), in which the model is nudged by the MERRA meteorological fields (Rienecker et al., 2011) from January 2004 to December 2011 (hereafter we only use WACCM to represent SD-WACCM4).

Figure 2 shows the annual zonal mean ratio of net tendency (production rate minus loss rate) divided by the loss rate for O_x and CO. These show the mean differences of production to loss, with positive numbers indicating net chemical increase and negative numbers indicating net chemical decrease; values close to zero imply balanced production vs. loss. In the background are the respective photochemical lifetimes evaluated from the loss rates ($\tau_L = [\chi]/L_\chi$). Both O_x and CO exhibit relatively long lifetimes (> 3 months) in the lower–middle stratosphere, and hence transport will have a dominant influence on their distributions. Above $\sim 30\,km$ the lifetimes are shorter, and the photochemical behavior will determine chemical structure.

Here O_x is the odd oxygen – the sum of O_3 and O. We use the production and loss rates of O_x because (1) the time step of trajectory model is 1 day, which is much longer than the lifetime of O_3 in the middle and upper stratosphere, and (2) the abundances of O_3 only change on timescales comparable to or longer than the lifetime of O_x (see, e.g., Dessler, 2000, Chap. 3). Therefore, it is reasonable to use production and loss rate of O_x instead of O_3 for our purpose of simulation. Because O_3 abundance is much greater than O – i.e., $O_x \approx O_3$ – throughout the rest of the paper we use O_3 and O_x interchangeably.

O_x production in the stratosphere is almost entirely due to the photolysis of O_2. P_{O_x} increases with altitude over most of the stratosphere because the photolysis rate (proportional
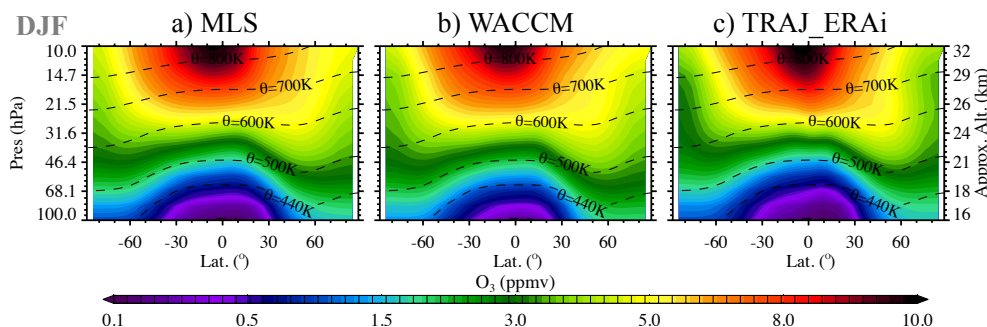
Figure 3. Trajectory modeled O_3 driven by ERAi reanalysis wind (**c**, TRAJ_ERAi) in boreal winter (DJF), compared to both MLS observations (**a**) and WACCM output (**b**). Both WACCM and trajectory model results are weighted by the MLS averaging kernels. Dashed lines are potential temperature contours, demonstrating that in the lower stratosphere where transport dominates, chemical distributions roughly follow the isentropes.

to solar radiation) increases faster with altitude than $[O_2]$ decreases, so the net effect is increasing. Figure 2a shows that from 150 to ~ 10 hPa O_x production exceeds loss in the tropics, whereas a net chemical decrease of O_3 occurs in mid- to high latitudes (transport of O_3 from the tropics to higher latitudes closes the budget). Between about 10 and 2 hPa the daily production and loss of O_x become comparable and the system is in diurnal steady state. The system gradually reaches photochemical steady states above ~ 2 hPa, where the lifetime of O_x is less than a day and the instantaneous production and loss can be treated equally throughout the day. Here we simply set the $[O_x]$ to be (P_{O_x}/LF_{O_x}) in our trajectory calculations.

In the UTLS region, the main source of CO is from the troposphere (from direct emissions and photochemical production), and this source is accounted for by initializing trajectories with observed values of CO. There is a net chemical decrease (Fig. 2b) in the UTLS, where CO is predominantly removed by oxidation with OH. CO experiences a net increase in the middle stratosphere (above ~ 24 km) due to oxidation of methane (CH_4), although this has little influence on the results shown here.

In our simulation P_χ and LF_χ are calculated from WACCM as a function of latitude, altitude, and climatological months averaged over 2005–2011, so that a constant annual cycle is applied throughout the model integration. As discussed in Sect. 5, this calculation will not accurately handle the situation where chemical losses are linked to meteorological behavior, such as for ozone losses in the polar winter stratosphere.

2.3   MLS observations of O_3 and CO

We will compare the model to observations of O_3 and CO from the Aura MLS (Waters et al., 2006). MLS climatology (constant annual cycle) of O_3 and CO averaged from August 2004 to December 2012 is used to set the initial abundances when parcels are initialized at the 370 K level,

and the observations at higher levels are used to evaluate the trajectory model results. We use the MLS version 3.3 (v3.3) Level 2 products, described in the data quality and description document (http://mls.jpl.nasa.gov/data/v3-3_data_quality_document.pdf). O_3 profiles are available at 12 levels per decade from 261 to 0.02 hPa, and CO profiles are available between 215 and 0.0046 hPa at 6 levels per decade. The vertical resolution of O_3 in the UTLS is approximately 2.5–3 km while for CO it is ~ 4.5–5 km. The detailed validation for these data sets can be found in Froidevaux et al. (2008), Pumphrey et al. (2007), and Livesey et al. (2008).

For the comparisons shown here, we applied the MLS O_3 and CO averaging kernels to both our trajectory simulations and WACCM model outputs when comparing with the MLS observations. We have followed the detailed instructions for applying averaging kernels as described in http://mls.jpl.nasa.gov/data/v3-3_data_quality_document.pdf.

2.4   Other verifying data sets

Besides using chemical production and loss from WACCM, we also compare O_3 and CO modeled by WACCM to the trajectory model simulations, which serves as a sanity check of applying the imposed WACCM chemistry, and also as a simple comparison of Lagrangian vs. Eulerian model results. We also compare the trajectory modeling to the CO measurements from ACE-FTS (Bernath et al., 2005), which shows some systematic differences from MLS retrievals in the stratosphere (Clerbaux et al., 2008; Park et al., 2013). A detailed description of the ACE CO observations can be found in Park et al. (2013).

3   Trajectory modeling results

3.1 O_3 Results

Figure 3 shows the zonal mean cross section of O_3 during December–February (DJF) from the trajectory model
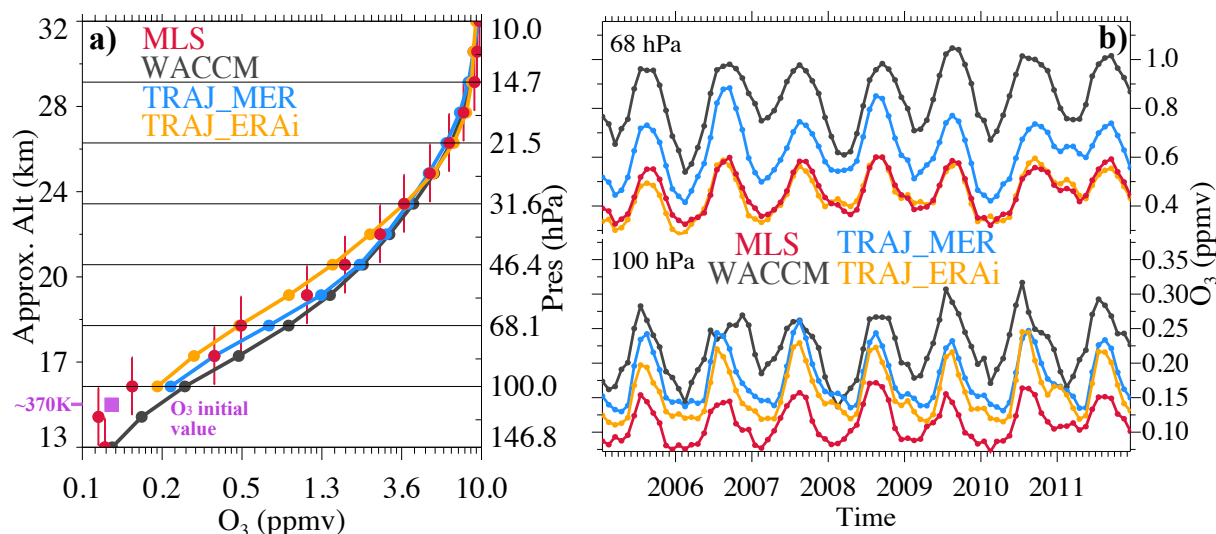
Figure 4. Tropical **(a)** vertical profile and **(b)** time series (100 hPa, bottom panel; 68 hPa, upper panel) of MLS, WACCM, and trajectory modeled O_3 driven by MERRA wind and ERAi wind, averaged over the deep tropics (18° N–18° S) from 2005 to 2011. Both WACCM and trajectory model results are weighted by the MLS averaging kernels. In **(a)** the x axis is in log scale to highlight the differences: the purple square indicates the initial O_3 values carried by parcels when they were first injected into the domain at 370 K; the vertical bars in red indicate the MLS vertical resolutions at each of the MLS retrieval pressure levels.

driven by ERAi reanalysis (denoted as "TRAJ_ERAi"), compared to both the MLS observations and the WACCM results. Because O_3 above 10 hPa is in photochemical steady state (Sect. 2) we focus on O_3 below 10 hPa. Overall the trajectory simulations agree with results from both MLS and WACCM. In the lower stratosphere transport plays an important role in re-distributing chemical species, resulting in contours of O_3 approximately following the isentropes. The enhanced O_3 production due to photolysis at 30 km ($\sim$ 10 hPa) shifts from south during DJF towards north during JJA (not shown), following the seasonal variations of photolysis rates.

Vertical profiles of O_3 averaged over the deep tropics (18° N–18° S) from 2005 to 2011 are shown in Fig. 4a (note that the x axis is in log scale). The trajectory model driven by MERRA (denoted as "TRAJ_MER") shows reasonable agreement with MLS data (and WACCM) in the lower stratosphere, while the results based on ERAi (denoted as "TRAJ_ERAi") show relatively smaller O_3 values. Above 24 km where photochemical processes dominate, different trajectory runs yield similar results and they both agree with MLS and WACCM data. Note that the MERRA and ERAi simulations use identical O_3 initial values at 370 K, so that the differences in Fig. 4a are primarily a result of differences in upward circulation (Fig. 1). The mean differences in ozone in the lower stratosphere can be explained as a result of the different heating rates (vertical circulations) imposed. The ERAi heating rates are higher than MERRA up to 20 km (Fig. 1). Due to the positive vertical gradient in O_3 the stronger circulation moves air with lower O_3 upward, creating a lower relative concentration compared to MERRA.

Monthly time series of O_3 at 100 and 68 hPa averaged over the deep tropics (18° N–18° S) are shown in Fig. 4b. There is a strong annual cycle in ozone at these levels related to the seasonal variations in tropical upwelling (Randel et al., 2007; Abalos et al., 2012, 2013a), and this behavior is reproduced by the trajectory model, showing reasonable agreement in amplitude with the MLS observations and WACCM results (in spite of the differences in mean values). There are somewhat larger differences in annual cycle amplitude at 68 hPa, with the ERAi trajectory results showing better agreement with MLS.

The simulated and observed latitudinal structure of zonal mean O_3 in the lower stratosphere (68 hPa) throughout the seasonal cycle is shown in Fig. 5. The overall variations are reasonably well simulated by the trajectory model, although low biases are found compared to MLS over middle-to-high latitudes in both hemispheres (and WACCM is systematically higher over the globe). The development of the Antarctic ozone hole is evident in the very low ozone values polewards of 60° S in October, which is simulated in the trajectory model based on the strong chemical ozone losses in this region derived from WACCM.

Figure 6 compares the horizontal structure of boreal summer (JJA) O_3 at 83 hPa from MLS data and the trajectory results driven by MERRA. The trajectory results show a reasonable simulation of the spatial patterns compared to MLS (and WACCM; not shown), with a clear minimum inside the Asian monsoon anticyclone linked to upward transport of ozone-poor air from lower levels (Park et al., 2009). There
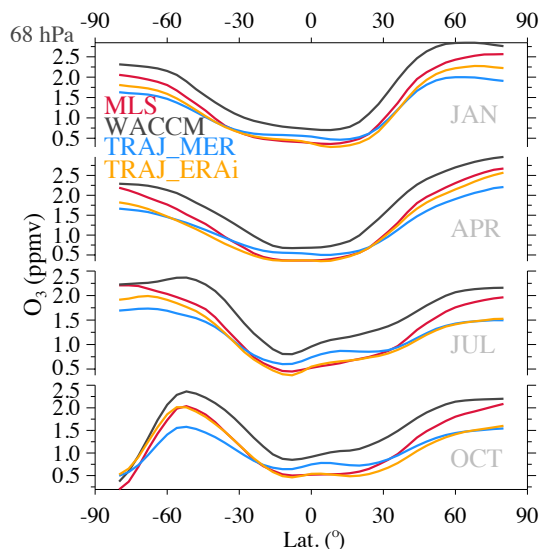
Figure 5. Zonal mean of O_3 at 68 hPa during January (JAN), April (APR), July (JUL), and October (OCT) averaged in 2005–2011 from MLS, WACCM, and trajectory results driven by MERRA wind and ERAi wind. Both WACCM and trajectory model results are weighted by the MLS averaging kernels. In October (Antarctic spring time), the South Pole undergoes exceptional depletion of O_3.

Figure 6. Northern Hemisphere summertime (JJA) tropical O_3 distributions at 83 hPa averaged from 2005 to 2011 between MLS and the MERRA-driven trajectory simulations (weighted by the MLS averaging kernels). Horizontal wind vectors from the MERRA reanalysis are overlaid to emphasize the Asian summer monsoon anticyclone.

is also relatively low O_3 centered near 15° S linked to the slow ascending air from the troposphere in this region.

The trajectory model is also able to capture the spatial behavior of polar ozone. Figure 7 shows a comparison of high-latitude O_3 in the Northern Hemisphere (NH) during winter (DJF) and in the Southern Hemisphere (SH) during spring (September) between MLS and trajectory modeling driven by both MERRA and ERAi winds. During NH winter, O_3-rich air (> 2.2 ppmv) occurs within the polar vortex (denoted with the 24 PVU isopleth in Fig. 7a–c), and the trajectory model captures the observed isolation from middle latitudes, although differences in magnitude exist. During SH springtime, the Antarctic ozone hole (denoted with the 195 K isotherm in Fig. 7d–f) is reasonably well reproduced in the trajectory model based on imposed WACCM chemistry. The trajectory model also captures the spatial structure of the zonal wave ozone maximum near 50° S (the so-called "ozone croissant"), linked to the descending branch of the Brewer–Dobson (BD) circulation. The weaker extravortex high in ozone in the trajectory model may be related to the weaker overall circulation in MERRA compared to observations (Schoeberl et al., 2012, 2013). Noted that due to the climatological loss frequency adopted from WACCM, this model cannot account for interactions of circulation and chemistry, which affects O_3 mostly in winter polar regions (see Sect. 5).
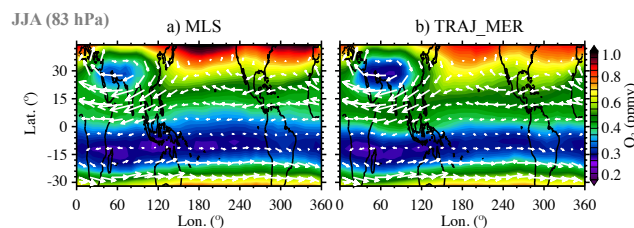
3.2 CO results

Figure 8 shows that zonal mean cross sections of CO from ACE-FTS, WACCM, and the trajectory model agree well in the lower stratosphere. Here, instead of sampling trajectory results at the ACE measurement locations, we only took zonal mean averages because, as mentioned in Park et al. (2013), the differences between two processing are negligible. CO has a maximum in the tropical upper troposphere, and decreases with altitude due to OH oxidation to a minimum near 22 km. CO increases above this altitude due to production from methane (CH_4) oxidation. The ACE-FTS observations show high CO mixing ratios in the polar middle and upper stratosphere regions, resulting from the downward transport of CO from the mesosphere (from photodissociation of CO_2); this behavior is also seen (to a weaker degree) in WACCM, but is not simulated in the trajectory model, which does not include mesospheric processes.

Figure 9a shows the CO vertical profiles and time series averaged in the deep tropics (15° N–15° S). Due to the differences of MLS and ACE-FTS retrievals in the stratosphere, here we also included ACE CO for comparison. The vertical profiles in Fig. 9a show broad-scale agreements, although there are differences among the trajectory models (with ERAi-driven results larger than those driven by MERRA) and also between the ACE-FTS and MLS observations (all of the models agree better with the ACE observations above 22 km). Time series of CO at 100 hPa (Fig. 9b) show a semi-annual cycle linked to initialized variations in the upper troposphere (Liu et al., 2007), with approximate agreement among the models and observations (with slightly larger values in the MLS data). The variability changes to an annual cycle at 68 hPa, as a response to variations in tropical upwelling. At 68 hPa the annual cycle is captured in a reasonable manner in the models, with the ERAi results showing better agreement with MLS and ACE-FTS data.

A further diagnostic to evaluate the model simulations is made by plotting monthly tropical (15° N–15° S) averages of O_3 vs. CO in the lower stratosphere (68 hPa), as shown in
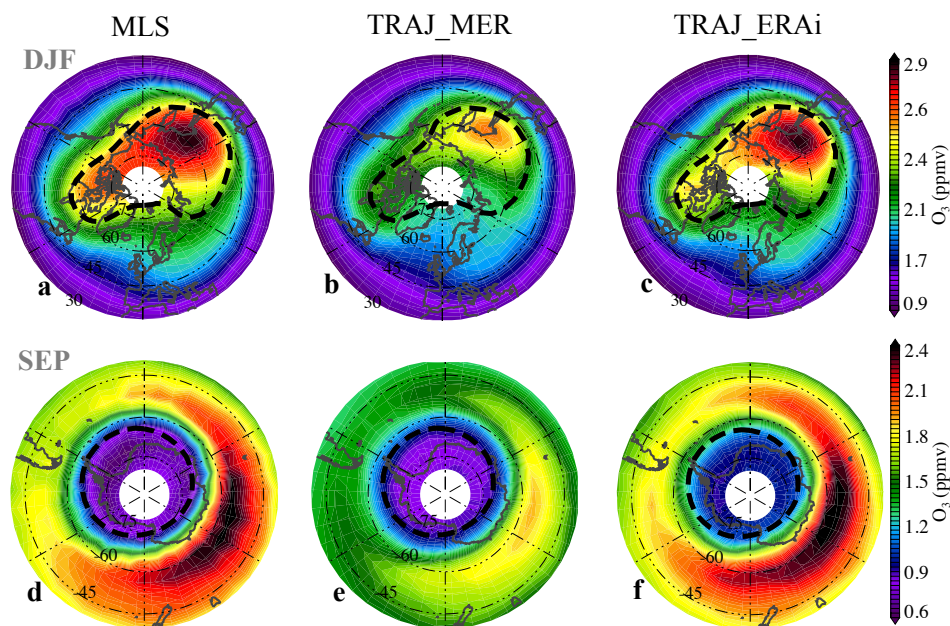
Figure 7. Polar O_3 distributions shown in MLS (left column), trajectory results driven by MERRA (middle column), and trajectory results driven by ERAi (right column) during Northern Hemisphere winter (DJF, **a–c**) and Southern Hemisphere spring (September, SEP, **d–f**) at 68 hPa. Trajectory results are weighted by the MLS averaging kernels. The 24 PVU potential vorticity level (**a–c**) and the 195 K temperature (**d–f**) are overlaid in black dashed lines for DJF and SEP, respectively.
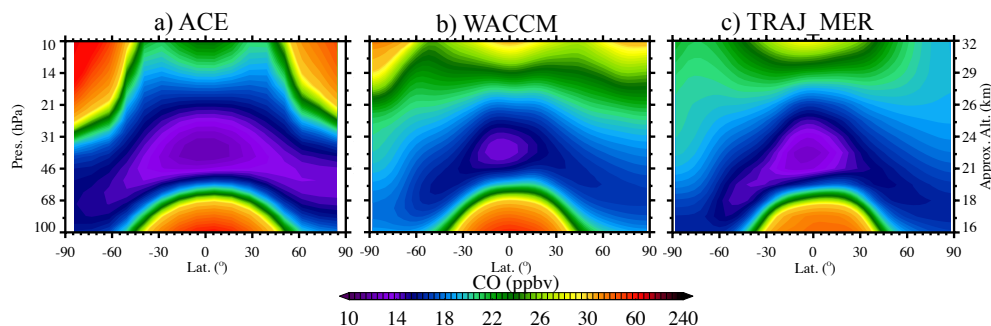

Figure 8. Zonal mean cross sections of CO from (**a**) ACE-FTS, (**b**) WACCM, and (**c**) trajectory model driven by MERRA reanalysis.

Fig. 10. This includes the observations from MLS, together with trajectory model simulations driven by both MERRA and ERAi, which show the sensitivity to different Q (see also Fig. 1). There is an overall anti-correlation between O_3 and CO in Fig. 10, mainly representing the out-of-phase annual cycles seen in Figs. 4b and 9b. The comparisons in Fig. 10 show that stronger upwelling in the ERAi simulation produces slightly lower values of O_3 and higher values in CO (> 30 ppbv), in better agreement with MLS data. Moreover, the slope of the CO–O_3 variations in the ERAi simulation approximately matches the MLS result.

The DJF and JJA seasonal distributions of CO at 68 hPa from the ERAi trajectory model are compared to MLS data in Fig. 11. In both seasons the trajectory model shows spatial patterns consistent with MLS data. During DJF the pat-

terns show a center of high CO over Central America and enhancements over southeastern Asia, extending to the tropical western Pacific (largely attributable to fossil fuel emissions; Jiang et al., 2007). The trajectory model also captures the well-known CO maximum linked to the Asian monsoon anticyclone during JJA, which is substantially stronger at the 100 hPa level (e.g., Randel and Park, 2006; Park et al., 2009; Randel et al., 2010).

Overall, the large-scale seasonal behavior of CO simulated by the trajectory model is in agreement with both observations (MLS and ACE-FTS) and Eulerian chemical model (WACCM), although the results are sensitive to the tropical upwelling speed (see Sect. 5).
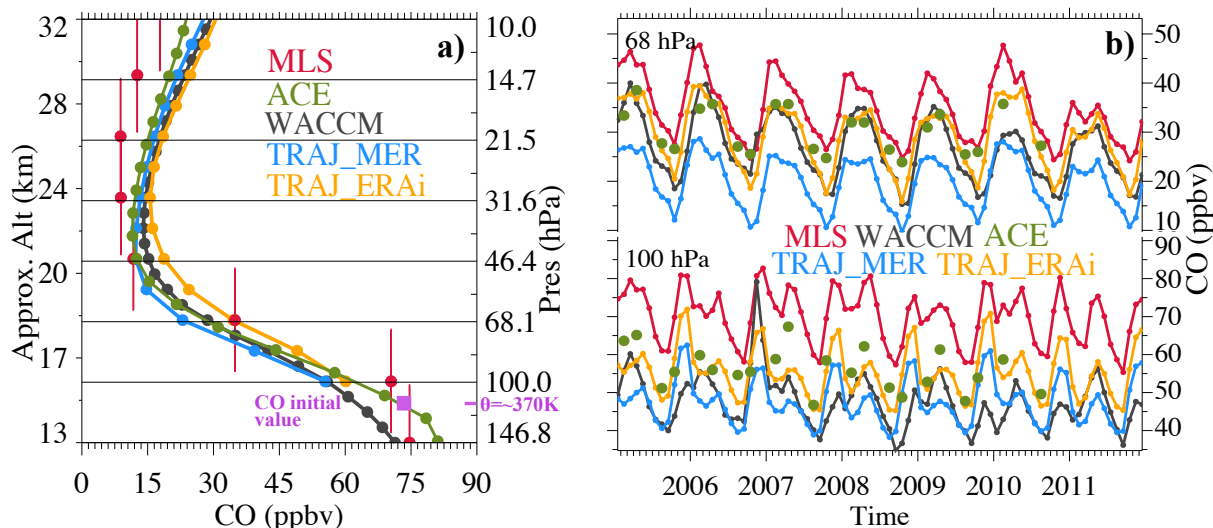
Figure 9. Tropical (**a**) vertical profile and (**b**) time series (100 hPa, bottom panel; 68 hPa, upper panel) of MLS, WACCM, ACE, and trajectory modeled CO driven by MERRA wind and ERAi wind, averaged over 15° N–15° S from 2005 to 2011. In (**b**) the WACCM and trajectory model results are weighted by the MLS averaging kernels. In (**a**) the purple square indicates the initial CO values carried by parcels when they were first injected into the domain at 370 K, and vertical bars in red indicate the MLS vertical resolutions at each of the MLS retrieval pressure levels.
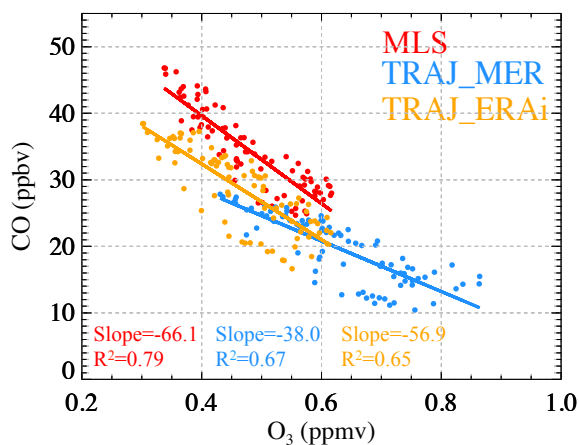

Figure 10. Monthly variations of O$_3$ vs. CO in the tropical lower stratosphere (15° N–15° S, 68 hPa) from MLS and trajectory modeling driven by MERRA wind and ERAi wind. Trajectory results are weighted by the MLS averaging kernels.

Figure 11. Comparison of CO at 68 hPa ($\sim$ 20 km) during DJF (top row, **a** and **b**) and JJA (bottom row, **c** and **d**) between MLS (left) and trajectory modeling driven by ERAi wind (right, weighted by the MLS averaging kernels). Horizontal wind vectors from ERAi are overlaid as reference.

4 Interannual variability of tracers in the tropical lower stratosphere

The coherent seasonal variations in O$_3$ and CO in the tropical lower stratosphere demonstrate that transport processes have a large impact on the chemical concentrations in this region. The Eulerian-mean calculations of Abalos et al. (2012, 2013a) show that tropical upwelling is the main driver of the annual cycles in O$_3$ and CO above the tropical tropopause. Our Lagrangian trajectory model results (Figs. 4b and 9b)
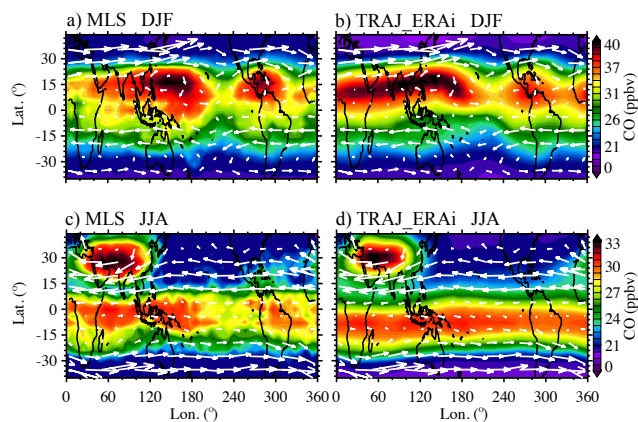
also show that the annual cycles of O$_3$ and CO above the tropopause (especially around 70 hPa) are strongly influenced by the tropical upwelling (Brewer–Dobson) circulation.

We further explore interannual variations in the chemical tracers and links to changes in the upwelling circulation. Figure 12 shows the interannual anomalies (by removing the annual cycle) in O$_3$ and CO concentrations in the tropical lower stratosphere from MLS observations and from trajectory calculations, and in addition anomalies in diabatic
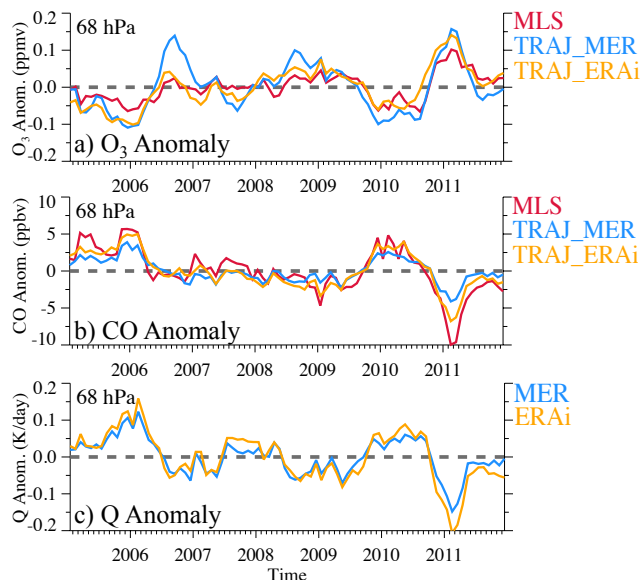
Figure 12. Interannual anomalies of **(a)** O_3 and **(b)** CO from MLS (red) and trajectory simulations driven by MERRA and ERAi in the tropical ($15°$ N–$15°$ S) lower stratosphere (68 hPa). **(c)** shows interannual anomalies of total diabatic heating rates from MERRA and ERAi, which serves in our model as the vertical velocity. The trajectory results are weighted by the MLS averaging kernels.

heating rates (upwelling) from reanalysis at 68 hPa. While there are significant differences in time-mean diabatic heating rates between MERRA and ERAi (Fig. 1), interannual changes in Q (Fig. 12c) show good agreement. Figure 12 shows that interannual anomalies in O_3 and CO are strongly anti-correlated (due to oppositely signed vertical gradient) and closely linked to interannual changes in diabatic heating. Furthermore, Fig. 12 shows that trajectory calculations driven by both MERRA and ERAi are able to simulate the observed interannual anomalies in O_3 and CO, in spite of significant differences for the background seasonal cycle (Fig. 4b and 9b).

Taking results from the MERRA run as an example, the close relationship between anomalies in diabatic heating and O_3 is quantified in Fig. 13a, which shows strong anti-correlation with explained variance $r^2 = 0.73$ and slope $\Delta O_3 / \Delta Q = -1.05 \pm 0.14$ (ppmv)/(K day^{-1}). Similar strong correlation is found for CO and Q anomalies (Fig. 13b), with explained variance $r^2 = 0.85$ and slope of 31.11 ± 2.86 (ppbv)/(K day^{-1}). The signs of the slopes in Fig. 13a–b are opposite because of the different background vertical gradients for O_3 and CO. These strong relationships between diabatic heating (Q) and tracer anomalies highlight the dominant role of tropical upwelling in controlling species with strong vertical gradients near the tropical tropopause.

Figure 12 also highlights strong anti-correlations between O_3 and CO anomalies, which is further demonstrated in Fig. 13c. Abalos et al. (2012) have shown that for the ide-

alized case where upwelling dominates tracer transports, the ratio of tendencies for two tracers (χ_1, χ_2) is closely related to the ratio of the respective background gradients:

$$\frac{\partial \overline{\chi}_1}{\partial t} / \frac{\partial \overline{\chi}_2}{\partial t} = \frac{\partial \overline{\chi}_1}{\partial z} / \frac{\partial \overline{\chi}_2}{\partial z} \quad \sim \quad \text{constant.} \qquad (2)$$

Integrating this equation in time for monthly O_3 and CO anomalies gives the relationship

$$\Delta \overline{O_3} / \Delta \overline{CO} \approx \frac{\partial \overline{O_3}}{\partial z} / \frac{\partial \overline{CO}}{\partial z}; \qquad (3)$$

i.e., the ratio of monthly anomalies approximately follows the ratio of background vertical gradients for the idealized situation where vertical transport is dominant. For the case of CO and O_3 in the tropics near 68 hPa, the MERRA trajectory results yield a background gradient ratio of ~ -18.34 (ppbv km^{-1})/(ppmv km^{-1}) for (dCO/dz)/(dO_3/dz). A linear fit of the observed CO / O_3 anomalies (Fig. 13c) gives a ratio of -22.45 ± 3.40 (ppbv / ppmv), which is close to the idealized result (slightly outside of the two-sigma uncertainty). This approximate agreement with highly idealized theory provides further evidence for the control of tropical lower stratosphere O_3 and CO by variations in upwelling.

5 Summary and discussion

The results presented here demonstrate that the domain-filling, forward trajectory model is useful for studying the transport of trace gases in the lower stratosphere. The O_3 and CO simulations are complementary to modeling H_2O (mainly controlled by tropopause temperature) in that O_3 and CO rely on both initial conditions and chemical production and loss rates, and are sensitive to transport. Initial conditions based on observations provide entry values of chemical species into the lower stratosphere; after that the chemical production and loss control the net changes of concentrations along the trajectories. Because the MERRA negative heating rates at 150–130 hPa (Fig. 1) prevent air ascending to the stratosphere, we chose a relatively high initialization level in the upper troposphere (370 K) in this study. However, we could have initiated parcels at lower altitude, such as 355 K when using ERAi circulation, to extend the results to the upper troposphere.

Trajectory modeled O_3 and CO in the tropical lower stratosphere largely depend on the strength of upwelling (and to a lesser degree on the amount of mixing with extratropics; Abalos et al., 2013a). Stronger upwelling is linked to faster transport, which results in less time for chemical production (for O_3) or loss (for CO), leading to overall lower values of O_3 (Fig. 4a) and higher values of CO (Fig. 9a). The comparisons of MERRA and ERAi simulations that have different tropical upwelling rates (Q), e.g., Fig. 1, clearly demonstrate this sensitivity. The detailed differences in diabatic heating rates among reanalyses have been discussed
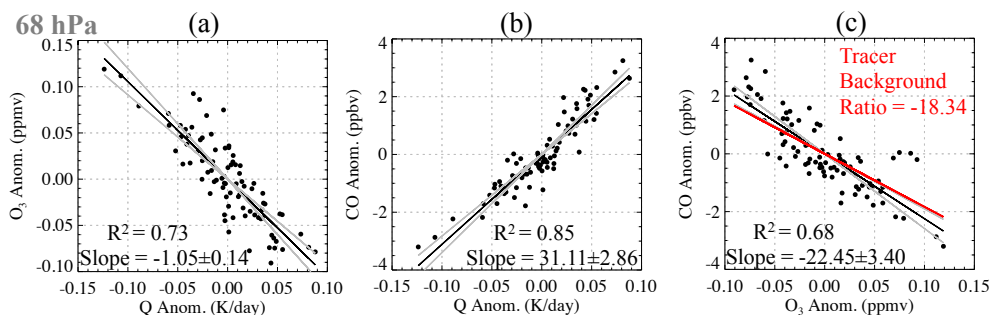
Figure 13. Scatter plots of the anomalies of **(a)** O$_3$ vs. Q, **(b)** CO vs. Q, and **(c)** CO vs. O$_3$ at 68 hPa. The dots are monthly variations of tracers from trajectory modeling driven by MERRA winds and diabatic heating rates; the black lines show the linear fit. The red line in **(c)** is the theoretically estimated tracer ratio estimated from the respective background gradients, using simplified relation in Eq. (3).

by Wright and Fueglistaler (2013), who highlight differences in the corresponding long-wave radiative heating rates in the lower stratosphere, which are influenced by both temperature and ozone. We also conducted a sensitivity study of increasing MERRA diabatic heating rates (Q) by constant factors, and the best overall fit to the observations is 1.5 times the MERRA Q values, consistent with the ERAi-based results.

Although better agreement with observations of CO in the tropical lower stratosphere is found using ERAi data, there is reason to suspect that the ERAi diabatic heating in this region may be too high. For example, Ploeger et al. (2012) performed a radiative calculation showing that ERAi heating rates are $\sim 40\%$ too high, consistent with Schoeberl et al. (2012), who show that trajectory modeled water vapor tape recorder signal based on ERAi heating rates is $\sim 30\%$ too fast compared with MLS observations. In spite of the detailed differences, the trajectory modeled O$_3$ shows reasonable simulation of the large-scale seasonal structure compared to both MLS and WACCM, including both the tropics and the polar regions. The trajectory modeled CO in the tropical stratosphere is more sensitive to the MERRA vs. ERAi differences, likely because of the shorter photochemical lifetime of CO in the lower stratosphere compared to O$_3$.

The annual cycles in O$_3$ and CO in the tropical lower stratosphere are reproduced in the trajectory model simulations, and the magnitude of variations provides a useful test of the imposed circulation. The variability of O$_3$ and CO shows significant correlations with fluctuations in diabatic heating, for both seasonal and interannual timescales. These close relationships support the concept that tropical upwelling plays a key role in regulating variability for chemical species with strong vertical gradients in the lower stratosphere (and explains the observed compact relationships among interannual anomalies in diabatic heating, O$_3$, and CO seen in Figs. 12–13). For the idealized situation where upwelling dominates tracer transports, the tracer ratios can be expressed as ratios of the background vertical gradients, and the observed O$_3$ and CO changes are in approximate agreement with this expectation (Fig. 13c).

The discussion above linking seasonal or interannual changes in O$_3$ and CO with chemical changes along slower or faster upward trajectories is a Lagrangian perspective on transport (appropriate for our Lagrangian trajectory model). In contrast, the discussion linking O$_3$ and CO variations at particular pressure levels to varying circulations acting on background vertical gradients (Sect. 4) is an Eulerian perspective. These two perspectives are complementary and do not contradict each other; Abalos et al. (2013b) have recently shown the equivalence of Lagrangian and Eulerian transport calculations in the tropical lower stratosphere, highlighting that each can provide useful information.

One limitation of this model is that it cannot account for interactions of circulation and chemistry, due to the climatological chemical production rates and loss frequencies adopted from WACCM (Sect. 2.2). This is most likely important in winter polar regions, where O$_3$ loss chemistry due to chlorine activation on polar stratospheric clouds is highly temperature dependent. Although we cannot simulate the detailed behavior in any particular (cold) year with climatological chemical ozone loss rates, our model does a reasonable job at simulating the time-average behavior of polar regions.

Our simulations with O$_3$ and CO have demonstrated the viability of the domain-filling forward trajectory model for simulating species with relatively simple chemistry, and extension to other species would be straightforward. There are several potential applications for such a trajectory model, including describing parcel histories that characterize different transport pathways, and evaluating the importance of tropical–extratropical exchanges. For example, trajectories can allow tracing the sources of CO-rich air in the summertime Asian monsoon region, and quantifying the fate of the parcels after breakup of the anticyclone. The model can also allow detailed comparisons of transport based on different and new reanalysis data sets, or idealized studies of the chemical responses to UTLS circulation in a changing climate.

References

Abalos, M., Randel, W. J., and Serrano, E.: Variability in upwelling across the tropical tropopause and correlations with tracers in the lower stratosphere, Atmos. Chem. Phys., 12, 11505–11517, doi:10.5194/acp-12-11505-2012, 2012.

Abalos, M., Randel, W. J., Kinnison, D. E., and Serrano, E.: Quantifying tracer transport in the tropical lower stratosphere using WACCM, Atmos. Chem. Phys., 13, 10591–10607, doi:10.5194/acp-13-10591-2013, 2013a.

Abalos, M., Ploeger, F., Konopka, P., Randel, W. J., and Serrano, E.: Ozone seasonality above the tropical tropopause: reconciling the Eulerian and Lagrangian perspectives of transport processes, Atmos. Chem. Phys., 13, 10787–10794, doi:10.5194/acp-13-10787-2013, 2013b.

Andrews, D. G., Holton, J. R., and Leovy, C. B.: Middle Atmosphere Dynamics, Academic Press, Orlando, Florida, 489 pp., 1987.

Bernath, P. F., McElroy, C. T., Abrams, M. C., Boone, C. D., Butler, M., Camy-Peyret, C., Carleer, M., Clerbaux, C., Coheur, P. F., Colin, R., DeCola, P., Maziere, M. D., Drummond, J. R., Dufour, D., Evans, W. F. J., Fast, H., Fussen, D., Gilbert, K., Jennings, D. E., Llewellyn, E. J., Lowe, R. P., Mahieu, E., McConnell, J. C., McHugh, M., McLeod, S. D., Michaud, R., Midwinter, C., Nassar, R., Nichitu, F., Nowlan, C., Rinsland, C. P., Rochon, Y. J., Rowlands, N., Semeniuk, K., Simon, P., Skelton, R., Sloan, J. J., Soucy, M. A., Strong, K., Tremblay, P., Turnbull, D., Walker, K. A., Walkty, I., Wardle, D. A., Wehrle, V., Zander, R., and Zou, J.: Atmospheric Chemistry Experiment (ACE): mission overview, Geophys. Res. Lett., 32, L15S01, doi:10.1029/2005GL022386, 2005.

Bowman, K. P.: Large-scale isentropic mixing properties of the Antarctic polar vortex from analyzed winds, J. Geophys. Res., 98, 23013–23027, 1993.

Bowman, K. P.: Transport of carbon monoxide from the tropics to the extratropics, J. Geophys. Res., 111, D02107, doi:10.1029/2005JD006137, 2006.

Bowman, K. P. and Carrie, G. D.: The mean-meridional transport circulation of the troposphere in an idealized GCM, J. Atmos. Sci., 59, 1502–1514, 2002.

Bowman, K. P., Lin, J. C., Stohl, A., Draxler, R., Konopka, P., Andrews, A., and Brunner, D.: Input data requirements Lagrangian Trajectory Models, B. Am. Meteorol. Soc., 94, 1051–1058, doi:10.1175/BAMS-D-12-00076.1, 2013.

Clerbaux, C., George, M., Turquety, S., Walker, K. A., Barret, B., Bernath, P., Boone, C., Borsdorff, T., Cammas, J. P., Catoire, V., Coffey, M., Coheur, P.-F., Deeter, M., De Mazière, M., Drummond, J., Duchatelet, P., Dupuy, E., de Zafra, R., Eddounia, F., Edwards, D. P., Emmons, L., Funke, B., Gille, J., Griffith, D. W. T., Hannigan, J., Hase, F., Höpfner, M., Jones, N., Kagawa, A., Kasai, Y., Kramer, I., Le Flochmoën, E., Livesey, N. J., López-Puertas, M., Luo, M., Mahieu, E., Murtagh, D., Nédélec, P., Pazmino, A., Pumphrey, H., Ricaud, P., Rinsland, C. P., Robert, C., Schneider, M., Senten, C., Stiller, G., Strandberg, A., Strong, K., Sussmann, R., Thouret, V., Urban, J., and Wiacek, A.: CO measurements from the ACE-FTS satellite instrument: data analysis and validation using ground-based, airborne and spaceborne observations, Atmos. Chem. Phys., 8, 2569–2594, doi:10.5194/acp-8-2569-2008, 2008.

Dee, D. P., Uppala, S. M., Simmons, A. J., Berrisford, P., Poli, P., Kobayashi, S., Andrae, U., Balmaseda, M. A., Balsamo, G., Bauer, P., Bechtold, P., Beljaars, A. C. M., van de Berg, L., Bidlot, J., Bormann, N., Delsol, C., Dragani, R., Fuentes, M., Geer, A. J., Haimberger, L., Healy, S. B., Hersbach, H., Hólm, E. V., Isaksen, L., Kållberg, P., Köhler, M., Matricardi, M., McNally, A. P., Monge-Sanz, B. M., Morcrette, J.-J., Park, B.-K., Peubey, C., de Rosnay, P., Tavolato, C., Thépaut, J.-N., and Vitart, F.: The ERA-Interim reanalysis: configuration and performance of the data assimilation system, Q. J. Roy. Meteor. Soc., 137, 553–597, doi:10.1002/qj.828, 2011.

Dessler, A. E.: A reexamination of the "stratospheric fountain" hypothesis, Geophys. Res. Lett., 25, 4165–4168, doi:10.1029/1998GL900120, 1998.

Dessler, A. E.: The Chemistry and Physics of Stratospheric Ozone, International Geophysics Series, Vol. 74, Academic Press, San Diego, 221 pp., 2000.

Dessler, A. E., Schoeberl, M. R., Wang, T., Davis, S. M., and Rosenlof, K. H.: Stratospheric water vapor feedback, P. Natl. Acad. Sci. USA, 110, 18087–18091, doi:10.1073/pnas.1310344110, 2013.

Fischer, H., Wienhold, F. G., Hoor, P., Bujok, O., Schiller, C., Siegmund, P., Ambaum, M., Scheeren, H. A., and Lelieveld, J.: Tracer correlations in the northern high latitude lower- 20 most stratosphere: influence of cross-tropopause mass exchange, Geophys. Res. Lett., 27, 97–100, doi:10.1029/1999GL010879, 2000.

Folkins, I., Braun, C., Thompson, A. M., and Witte, J.: Tropical ozone as an indicator of deep convection, J. Geophys. Res., 107, 1–10, doi:10.1029/2001JD001178, 2002.

Froidevaux, L., Jiang, Y. B., Lambert, A., Livesey, N. J., Read, W. G., Waters, J. W., Browell, E. V., Hair, J. W., Avery, M. A., Mcgee, T. J., Twigg, L. W., Sumnicht, G. K., Jucks, K. W., Margitan, J. J., Sen, B., Stachnik, R. A., Toon, G. C., Bernath, P. F., Boone, C. D., Walker, K. A., Filipiak, M. J., Harwood, R. S., Fuller, R. A., Manney, G. L., Schwartz, M. J., Daffer, W. H., Drouin, B. J., Cofield, R. E., Cuddy, D. T., Jarnot, R. F., Knosp, B. W., Perun, V. S., Snyder, W. V., Stek, P. C., Thurstans, R. P., and Wagner, P. A.: Validation of Aura Microwave Limb Sounder stratospheric ozone measurements, J. Geophys. Res., 113, D15S20, doi:10.1029/2007JD008771, 2008.

Fueglistaler, S., Bonazzola, M., Haynes, P. H., and Peter, T.: Stratospheric water vapor predicted from the Lagrangian temperature history of air entering the stratosphere in the tropics, J. Geophys. Res., 110, D08107, doi:10.1029/2004JD005516, 2005.

Fueglistaler, S., Dessler, A. E., Dunkerton, T. J., Folkins, I., Fu, Q., and Mote, P. W.: The tropical tropopause layer, Rev. Geophys., 47, RG1004, doi:10.1029/2008RG000267, 2009.

Garcia, R. R., Marsh, D. R., Kinnison, D. E., Boville, B. A., and Sassi, F.: Simulation of secular trends in the middle atmosphere, 1950–2003, J. Geophys. Res., 112, D09301, doi:10.1029/2006JD007485, 2007.

Jiang, J. H., Livesey, N. J., Su, H., Neary, L., McConnell, J. C., and Richards, N. A. D.: Connecting surface emissions, convective uplifting, and long-range transport of carbon monoxide in the upper troposphere: new observations from the Aura Microwave Limb Sounder, Geophys. Res. Lett., 34, L18812, doi:10.1029/2007GL030638, 2007.

Lamarque, J.-F., Emmons, L. K., Hess, P. G., Kinnison, D. E., Tilmes, S., Vitt, F., Heald, C. L., Holland, E. A., Lauritzen, P. H., Neu, J., Orlando, J. J., Rasch, P. J., and Tyndall, G. K.: CAM-chem: description and evaluation of interactive atmospheric chemistry in the Community Earth System Model, Geosci. Model Dev., 5, 369–411, doi:10.5194/gmd-5-369-2012, 2012.

Liu, C., Zipser, E., Garrett, T., Jiang, J. H., and Su, H.: How do the water vapor and carbon monoxide "tape recorders" start near the tropical tropopause?, Geophys. Res. Lett., 34, L09804, doi:10.1029/2006GL029234, 2007.

Liu, Y. S., Fueglistaler, S., and Haynes, P. H.: Advection-condensation paradigm for strato- spheric water vapor, J. Geophys. Res., 115, D24307, doi:10.1029/2010jd014352, 2010.

Livesey, N. J., Filipiak, M., Froidevaux, L., Read, W. G., Lambert, A., Santee, M. L., Jiang, J. H., Pumphrey, Hugh, Waters, J. W., Cofield, R. E., Cuddy, D. T., Daffer, W. H., Drouin, B. J., Fuller, R. A., Jarnot, R. F., Jiang, Y. B., Knosp, B. W., Li, Q. B., Perun, V. S., Schwartz, M. J., Snyder, W. V., Stek, P. C., Thurstans, R. P., Wagner, P. A., Avery, M., Browell, E. V., Cammas, J. -P., Christensen, L. E., Diskin, G. S., Gao, R.-S., Jost, H.-J., Loewenstein, M., Lopez, J. D., Nedelec, P., Osterman, G. B., Sachse, G. W., and Webster, C. R.: Validation of Aura Microwave Limb Sounder O$_3$ and CO observations in the upper troposphere and lower stratosphere, J. Geophys. Res., 113, D15S02, doi:10.1029/2007JD008805, 2008.

Logan, J., Prather, M., Wofsy, S., and McElroy, M.:. Tropospheric chemistry: a global perspective, J. Geophys. Res., 86, 7210–7254, doi:10.1029/JC086iC08p07210, 1981.

Mote, P. W., Rosenlof, K. H., McIntyre, M. E., Carr, E. S., Gille, J. C., Holton, J. R., Kinnersley, J. S., Pumphrey, H. C., Russell III, J. M., and Waters, J. W.: An atmospheric tape recorder: the imprint of tropical tropopause temperatures on stratospheric water vapor, J. Geophys. Res., 101, 3989–4006, 1996.

Park, M., Randel, W. J., Emmons, L. K., and Livesey, N. J.: Transport pathways of carbon monoxide in the Asian summer monsoon diagnosed from Model of Ozone and Related Tracers (MOZART), J. Geophys. Res., 114, D08303, doi:10.1029/2008JD010621, 2009.

Park, M., Randel, W. J., Kinnison, D. E., Emmons, L. K., Bernath, P. F., Walker, K. A., Boone, C. D., and Livesey, N. J.: Hydrocarbons in the upper troposphere and lower stratosphere observed from ACE-FTS and comparisons with WACCM, J. Geophys. Res.-Atmos., 118, 1964–1980, doi:10.1029/2012JD018327, 2013.

Ploeger, F., Konopka, P., Gunther, G., Grooss, J. U., and Muller, R.: Impact of the vertical velocity scheme on modeling transport in the tropical tropopause layer, J. Geophys. Res., 115, D03301, doi:10.1029/2009jd012023, 2010.

Ploeger, F., Konopka, P., Müller, R., Fueglistaler, S., Schmidt, T., Manners, J. C., Grooß, J.-U., Günther, G., Forster, P. M., and Riese, M.: Horizontal transport affecting trace gas seasonality in the Tropical Tropopause Layer (TTL), J. Geophys. Res., 117, D09303, doi:10.1029/2011JD017267, 2012.

Pumphrey, H. C., Filipiak, M. J., Livesey, N. J., Schwartz, M. J., Boone, C., Walker, K. A., Bernath, P., Ricaud, P., Barret, B., Clerbaux, C., Jarnot, R. F., Manney, G. L., and Waters, J. W.: Validation of middle-atmosphere carbon monoxide retrievals from the Microwave Limb Sounder on Aura, J. Geophys. Res., 112, D24S38, doi:10.1029/2007JD008723, 2007.

Randel, W. J. and Jensen, E. J.: Physical processes in the tropical tropopause layer and their role in a changing climate, Nat. Geosci., 6, 169–176, doi:10.1038/ngeo1733, 2013.

Randel, W. J. and Park, M.: Deep convective influence on the Asian summer monsoon anticyclone and associated tracer variability observed with Atmospheric Infrared Sounder (AIRS), J. Geophys. Res., 111, D12314, doi:10.1029/2005JD006490, 2006.

Randel, W., Park, M., Wu, F., and Livesey, N.: A large annual cycle in ozone above the tropical tropopause linked to the Brewer–Dobson Circulation, J. Atmos. Sci., 64, 4479–4488, 2007.

Randel, W. J., Park, M., Emmons, L., Kinnison, D., Bernath, P., Walker, K., Boone, C., and Pumphrey, H.: Asian monsoon transport of pollution to the stratosphere, Science, 328, 611–613, doi:10.1126/science.1182274, 2010.

Rienecker, M. M., Suarez, M. J., Gelaro, R., Todling, R., Bacmeister, J., Liu, E., Bosilovich, M. G., Schubert, S. D., Takacs, L., Kim, G.-K., Bloom, S., Chen, J., Collins, D., Conaty, A., da Silva, A., Gu, W., Joiner, J., Koster, R. D., Lucchesi, R., Molod, A., Owens, T., Pawson, S., Pegion, P., Redder, C. R., Reichle, R., Robertson, F. R., Ruddick, A. G., Sienkiewicz, M., and Woollen, J.: MERRA – NASA's modern-era retrospective analysis for research and applications, J. Climate, 24, 3624–3648, doi:10.1175/JCLI-D-11-00015.1, 2011.

Schoeberl, M. R. and Dessler, A. E.: Dehydration of the stratosphere, Atmos. Chem. Phys., 11, 8433–8446, doi:10.5194/acp-11-8433-2011, 2011.

Schoeberl, M. R., Douglass, A. R., Zhu, Z., and Pawson, S.: A comparison of the lower stratospheric age spectra derived from a general circulation model and two data assimilation systems, J. Geophys. Res., 108, 4113, doi:10.1029/2002JD002652, 2003.

Schoeberl, M. R., Duncan, B. N., Douglass, A. R., Waters, J., Livesey, N., Read, W., and Filipiak, M.: The carbon monoxide tape recorder, Geophys. Res. Lett., 33, L12811, doi:10.1029/2006GL026178, 2006.

Schoeberl, M. R., Douglass, A. R., Newman, P. A., Lait, L. R., Lary, D., Waters, J., Livesey, N., Froidevaux, L., Lambert, A., Read, W., Filipiak, M. J., and Pumphrey, H. C.: QBO and annual cycle variations in tropical lower stratosphere trace gases from HALOE and Aura MLS observations, J. Geophys. Res., 113, D05301, doi:10.1029/2007JD008678, 2008.

Schoeberl, M. R., Dessler, A. E., and Wang, T.: Simulation of stratospheric water vapor and trends using three reanalyses, Atmos. Chem. Phys., 12, 6475–6487, doi:10.5194/acp-12- 6475-2012, 2012.

Schoeberl, M. R., Dessler, A. E., and Wang, T.: Modeling upper tropospheric and lower stratospheric water vapor anomalies, Atmos. Chem. Phys., 13, 7783–7793, doi:10.5194/acp-13- 7783-2013, 2013.

Wang, T. and Dessler, A. E.: Analysis of cirrus in the tropical tropopause layer from CALIPSO and MLS data: a water perspective, J. Geophys. Res., 117, D04211, doi:10.1029/2011JD016442, 2012.

Waters, J. W., Froidevaux, L., Harwood, R. S., Jarnot, R. F., Pickett, H. M., Read, W. G., Siegel, P. H., Cofield, R. E., Filipiak, M. J., Flower, D. A., Holden, J. R., Lau, G. K. K., Livesey, N. J., Manney, G. L., Pumphrey, H. C., Santee, M. L., Wu, D. L., Cuddy, D. T., Lay, R. R., Loo, M. S., Perun, V. S., Schwartz, M. J., Stek, P. C., Thurstans, R. P., Boyles, M. A., Chandra, K. M., Chavez, M. C., Chen, G. S., Chudasama, B. V., Dodge, R., Fuller, R. A., Girard, M. A., Jiang, J. H., Jiang, Y. B., Knosp, B. W., LaBelle, R. C., Lam, J. C., Lee, K. A., Miller, D., Oswald, J. E., Patel, N. C., Pukala, D. M., Quintero, O., Scaff, D. M., Van Snyder, W., Tope, M. C., Wagner, P. A., and Walch, M. J.: The Earth Observing System Microwave Limb Sounder (EOS MLS) on the Aura satellite, IEEE T. Geosci. Remote, 44, 1075–1092, 2006.

Waugh, D. W. and Hall, T. M., Age of stratospheric air: theory, observations, and models, Rev. Geophys., 40, 1010, doi:10.1029/2000RG000101, 2002.

Winker, D. and Trepte, C.: Laminar cirrus observed near the tropical tropopause by LITE, Geophys. Res. Lett., 25, 3351–3354, 1998.

Wright, J. S. and Fueglistaler, S.: Large differences in reanalyses of diabatic heating in the tropical upper troposphere and lower stratosphere, Atmos. Chem. Phys., 13, 9565–9576, doi:10.5194/acp-13-9565-2013, 2013.